ChemComm

Accepted Manuscript

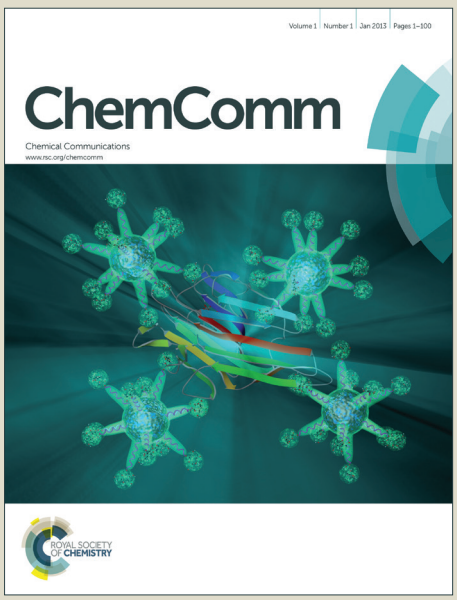

ROYAL SOCIETY OF CHEMISTRY

www.rsc.org/chemcomm

Journal Name

COMMUNICATION

Mesoporous $TiO_2/Zn_2Ti_3O_8$ Hybrid Films by Polymeric Micelle Assembly

Received 00th January 20xx,
Accepted 00th January 20xx

DOI: 10.1039/x0xx00000x

www.rsc.org/

Ming Zhao[a,b], Bishnu Prasad Bastakoti[c,f*], Yunqi Li[c,d], Hua Xu[a,b], Jinhua Ye[a,b,e], Zongwen Liu[f], and Yusuke Yamauchi[c,d*]

[a]TU-NIMS Joint Research Center, School of Materials Science and Engineering, Tianjin University, 92 Weijin Road, Nankai District, Tianjin 300072, P.R., China
[b]Collaborative Innovation Center of Chemical Science and Engineering (Tianjin), Tianjin 30072, P. R., China
[c]World Premier International (WPI) Research Center for Materials Nanoarchitectonics (MANA), National Institute for Materials Science (NIMS), 1-1 Namiki, Tsukuba, Ibaraki 305-0044, Japan
[d]Faculty of Science and Engineering, Waseda University 3-4-1 Okubo, Shinjuku, Tokyo 169-8555, Japan
[e]Environmental Remediation Materials Unit and International Center for Materials Nanoarchitectonics (WPI-MANA), National Institute for Materials Science (NIMS), 1-1 Namiki, Tsukuba 305-0044, Japan
[f] School of Chemical and Biomolecular Engineering, The University of Sydney, NSW 2006, Australia
bishnubastakoti@hotmail.com, *Yamauchi.Yusuke@nims.go.jp*
http://www.yamauchi-labo.com/

A hybrid mesoporous $TiO_2/Zn_2Ti_3O_8$ film with the pore size of around 40 nm is successfully synthesized by the polymeric micelles assembly approach. The chemically distinct units of polymeric micelles of poly(styrene-2-vinylpyridine-ethylene oxide) triblock copolymer simultaneously contribute to the formation of mesoporous $TiO_2/Zn_2Ti_3O_8$ films with enhanced photocatalytic activity during H_2 evolution reaction.

Semiconducting photocatalysis has been extensively investigated as one of the most promising technologies to ameliorate the situation of worsening environmental pollution and energy shortages. Since the photocatalytic reaction occurs on the surfaces of semiconductors, it is important to study the surface reaction to improve their surface conditions.[1-6] In recent years, synthesis of mesoporous (or nanoporous) materials has attracted great attention due to the large surface area of these materials, which provides more reactive sites during photocatalytic reactions.[7-11] Among the photocatalytic semiconducting materials, TiO_2 and ZnO have been widely studied due to their high photocatlytic activity, non-toxicity, low-cost, and easy preparation. However, the photocorrosion of ZnO restricts its uses in many applications. Homogeneous mixing of TiO_2 with ZnO overcomes the corrosion behavior of ZnO to some extent.[12-17] Dulin and Rase firstly established the basic phase diagram of ZnO-TiO_2 with cubic $Zn_2Ti_3O_8$, pure rhombohedral $ZnTiO_3$ and face-centered cubic Zn_2TiO_4.[18] $Zn_2Ti_3O_8$ is thermally stable with the cubic spinel-type structure, in which all of the Zn ions own the tetrahedral coordination, while all the Ti ions occupy octahedral coordinated sites.[9] The formation of $Zn_2Ti_3O_8$ prevents the rutile formation from anatase at elevated temperatures.[19] Modifying TiO_2 using heteroelements is one of the most important aspects to explore the catalytic activities of this catalyst. To the best of our knowledge, there are very few reports on the fabrication of mesoporous crystalline $Zn_2Ti_3O_8$.[20-22] Porous $Zn_2Ti_3O_8$ performs well in the photocatalytic water splitting with RuO_2, as co-catalyst.[23] The orderly arranged large-size mesoporous and crystalline materials with a $Zn_2Ti_3O_8$ phase have never been reported which are expected to be a novel catalyst.

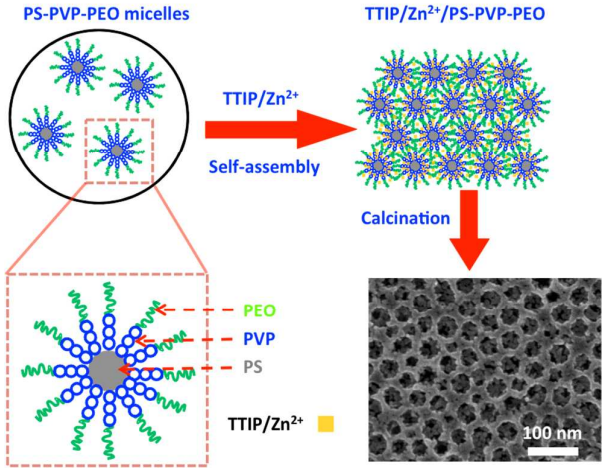

Fig. 1 Illustration of synthesis of mesoporous $TiO_2/Zn_2Ti_3O_8$ films by polymeric micelle assembly.

Here, we use the polymeric micelle of poly(styrene-2-vinylpyridine-ethylene oxide) (PS-PVP-PEO) to synthesize mesoporous $TiO_2/Zn_2Ti_3O_8$ films. The polymeric micelles of triblock copolymer have already been proved as an ideal template for preparing several mesostructure materials.[24-26] The chemically distinct units of polymeric micelles simultaneously contribute to forming the mesoporous $TiO_2/Zn_2Ti_3O_8$ films. The PS is a porogen,

and the PVP is a reaction site, while the PEO contributes the stabilization of micelles in the precursor solution. With increasing the phase fraction of $Zn_2Ti_3O_8$, the heterojunction between TiO_2 and $Zn_2Ti_3O_8$ increased, which highly enhanced the photocatalytic activity. However, on continuous increasing the portion of $Zn_2Ti_3O_8$, it seizes Ti atom from TiO_2, causing the decrease of heterojunction numbers and which leads to the decreasing of the catalytic efficiency. The effects of heterojunction and photocatalytic activity are discussed in detail.

In this experimental, the PS-PVP-PEO triblock copolymer (20 mg) was dissolved in THF (4 ml) under ultrasonic stirring to obtain a transparent solution at room temperature. HCl (80 μL, 35%) solution was slowly added into the solution to induce micellization and the mixed solution was magnetically stirred for 2 hours. TTIP (80 μL) and $Zn(NO_3)_2$ were separately dissolved in ethanol and sequentially added into the polymer solution with various mass ratios. The mass of $Zn(NO_3)_2$ was 0, 5, 10, 15 and 20 mg, which were denoted as ZTO0, ZTO5, ZTO10, ZTO15, and ZTO20, respectively. After 2 h stirring, the solution (200 μL) was used for spin coating on the clean silicon substrate or quartz substrate (2×2 cm), and the speed of spin coating was fixed at 3000 rpm for 30 s. The obtained films were dried for 12 hours at room temperature and calcined at 550 °C for 3 h with a ramping rate of 1 °C·min^{-1}. Pure mesoporous TiO_2 and $Zn_2Ti_3O_8$ films were also prepared for comparison.

To investigate the micellization of block copolymer, dynamic light scattering (DLS) measurement was performed. Before adding HCl solution, DLS did not detect any micelles or their aggregations. Block copolymer could be molecularly dissolved as unimers in THF, which is a good solvent for each block of polymer. The micellization was initiated by adding HCl solution, since it is a poor solvent for the PS block. The hydrodynamic diameter (D_h) of highly monodisperse micelles was around 110 nm. The pure polymeric micelles are positively charged with +30 mV zeta-potential. The optimal volume of HCl solution was fixed at 80 μL, which is enough to insolubilize the PS core and fully protonate the PVP block. The adequately protonated PVP block is the reaction site for inorganic precursors. After adding the inorganic species [TTIP and $Zn(NO_3)_2$], the D_h of the micelles decreased, since the interaction between the inorganic species and the PVP block initiated with charge neutralization, which further caused the alleviation of the electrostatic attraction between the adjacent PVP blocks. The zeta-potential measurement reveals that after adding TTIP the surface charge became almost zero (-1 mV). The micelles exhibit smaller diameter (85 ± 5 nm) than pure micelles (110 nm), indicating the shrunken conformation of the PVP blocks. Further addition of Zn^{2+} ions the hydrodynamic size remained unchanged. But the zeta-potential showed a positive value of + 24 mV indicating that the Zn^{2+} ions were strongly attached within the micelles composites. During evaporation of the solvent, the micelles assembled orderly as shown in **Fig. 1**.

To obtain the mesoporous films with opened pores, the polymer template was removed by thermal treatment, which also induced the crystallization of the inorganic framework. The PS-PVP-PEO block copolymer exhibits superior thermal stability compared with other block copolymers. The crystallization of the anatase TiO_2 phase is known to be initiated at around 300 °C[19] and the pure phase $Zn_2Ti_3O_8$ crystalized at around 500 °C.[22] Preserving the mesoporosity above their crystallization temperature is always important. The polymer used here decomposed completely at around 550 °C (**Fig. S1**). The remnant of *in-situ* formed carbon matrix can retard over crystal growth during calcination at high temperature, resulting in full retention of the mesostructure. The morphology of the mesoporous films with different compositions calcined at 550 °C were observed by SEM (**Fig. S2**). All the films contain large and uniform circular pores around 40 nm. The mesopores were surrounded by robust wall with a thickness of around 10 nm. With the increase of $Zn(NO_3)_2$ species, the uniform circular pores were gradually distorted and the mesoporous surface became rough (**Fig. S2a-S2e**). This is attributed to the formation of $Zn_2Ti_3O_8$ on the TiO_2 surface, which is discussed later. To investigate the internal structure of the mesoporous films, the TEM observation was carried out. Mesoporous structures surrounded by robust wall were formed over the entire area (**Fig. 2**). Elemental mapping data shows each element is uniformly distributed through the entire surface (**Fig. S3**). More details on the crystal structure were characterized by high-resolution TEM. Clear lattice fringes were observed on the walls (**Fig. 2b**). The distance of lattice fringes in the yellow circle was 0.350 nm corresponding to the (101) plane spacing of the anatase TiO_2 phase, while those in the red circle was 0.295 nm corresponding to the (220) plane spacing of the $Zn_2Ti_3O_8$ phase.

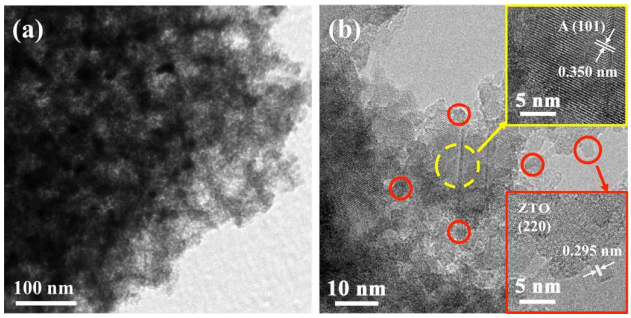

Fig. 2 TEM (a) and HRTEM images (b) of mesoporous film of ZTO15.

The crystallinity and phase purity were checked by wide angle XRD. The XRD patterns of the mesoporous films were indexed as the anatase TiO_2 (JCPDS no. 73-1764) and $Zn_2Ti_3O_8$ (JCPDS no. 87-1781), as shown in **Fig. S4**. The diffraction peaks at 25.34°, 37.96°, and 48.10° correspond to (101), (004), and (200) planes of the anatase TiO_2 phase, while the other peaks at 29.96 ° and 35.38° correspond to (220) and (311) of the $Zn_2Ti_3O_8$ phase, respectively. The phase content of the samples was calculated from the integrated intensities. The weight fraction of $Zn_2Ti_3O_8$ (W_{ZTO}) can be calculated from the following equation.

$W_{ZTO} = A_{ZTO}/(0.884A_A+A_{ZTO})$

where A_{ZTO} represents the integrated intensity of $Zn_2Ti_3O_8$ (311) peak, and A_A is the integrated intensity of the anatase (101) peak.[10, 11, 27] The phase compositions of the samples are summarized in **Table S1.** It is difficult to synthesize pure mesoporous $Zn_2Ti_3O_8$. According to ZnO-TiO_2 phase diagram, the $Zn_2Ti_3O_8$ and TiO_2 phases coexist stably below 800 °C.[28, 29] During calcination, the crystalline $Zn_2Ti_3O_8$ grows *in-situ* on the surface of anatase TiO_2.[8] However, mixed $Zn_2Ti_3O_8$/TiO_2 phase shows higher photocatalytic reactivity than pure $Zn_2Ti_3O_8$ due to the favourable carrier separation benefited the heterojunction structure.

The photocatalytic water splitting of H_2 evolution in presence of methanol was carried out to evaluate the photocatalytic activity of the mesoporous TiO_2/$Zn_2Ti_3O_8$ hybrid films (**Fig. 3a**). Each of the sample coating in the quartz substrate (2.0×2.0 cm) contains the same mass (0.1 mg) of catalyst. The photocatalytic activity is a surface reaction between the photocatalyst and the reactants, thus the heterojunction number has high impact on the photocatalytic

activity. The H_2 evolution rate was increased with increasing the amount of Zn amount. In this current work, ZTO15 achieved the optimal heterojunction condition and consequently exhibited the best H_2 evolution activity (**Table S1**). The heterojunction architecture contributes to the transfer of electrons that enhances the photocatalytic activity. The highest H_2 evolution activity of ZTO15 is attributed to higher $TiO_2/Zn_2Ti_3O_8$ heterojunction number. As shown in **Fig. 3b**, the photocatalytic process of $TiO_2/Zn_2Ti_3O_8$ heterojunction indicates that the photoelectron migrates from conduction band (CB) of TiO_2 to CB of $Zn_2Ti_3O_8$ and the photon hole transfers from valence band (VB) of $Zn_2Ti_3O_8$ to VB of TiO_2, therefore the recombination of carriers are greatly suppressed that improves the photocatalytic activity. The $Zn_2Ti_3O_8$ generated *in-situ* on the surface of TiO_2 forms $TiO_2/Zn_2Ti_3O_8$ heterojunction. With increasing the ratio of $Zn_2Ti_3O_8$ phase, the heterojunction between TiO_2 and $Zn_2Ti_3O_8$ gradually increased (ZTO0 to ZTO15). However, excess formation of $Zn_2Ti_3O_8$ probably seized the Ti from TiO_2, which decreased the amount of TiO_2 and reduced the heterojunction number. As a result of decreasing in heterojunction number in ZTO20, ultimately the evolution rate was also decreased. The role of mesoporosity on the photocatalytic reactivity was also studied (**Fig. S5**). ZTO15 exhibited better performance than the $TiO_2/Zn_2Ti_3O_8$ composite without mesospores. The mesoporosity decreases the distance of electron migration, which effectively reduce the recombination possibility of electrons and holes and further enhance the photocatalytic activity.

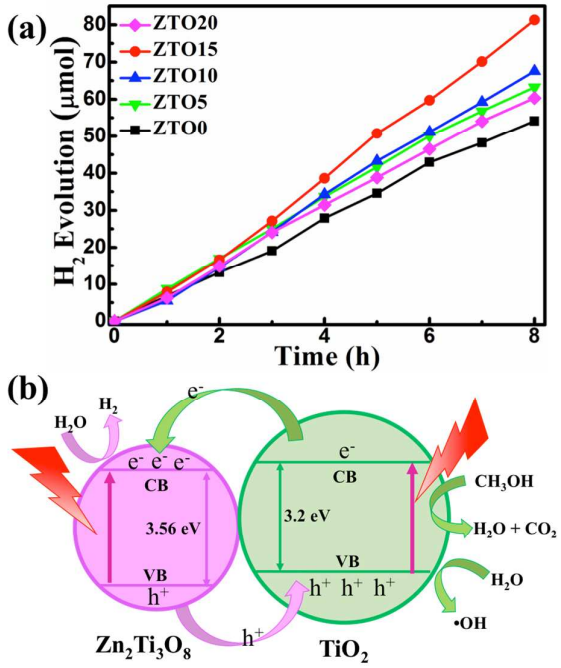

Fig. 3. (a) Comparison of photocatalytic activities for H_2 evolution of $TiO_2/Zn_2Ti_3O_8$ mesoporous thin films under UV-enhanced Xe lamp in presence of methanol. (b) Schematic illustration of the carriers migration of $TiO_2/Zn_2Ti_3O_8$ heterojunction.

To conclude, mesoporous $TiO_2/Zn_2Ti_3O_8$ hybrid films were successfully synthesized through the polymeric micelle assembly. Triblock copolymer (PS-PVP-PEO) with three chemically different blocks served as a smart template. By calcination at 550 ^{o}C, the polymeric template was completely removed to open the mesopores and the pore walls were well crystallized. Mesoporous architecture can provide more photocatalytic activity sites and shorten carrier transport distance. The increasing of the $Zn_2Ti_3O_8$ phase gradually increased the heterojunction between TiO_2 and $Zn_2Ti_3O_8$. However, the excess $Zn_2Ti_3O_8$ seized the Ti atom and weakened the heterojunction effects and thus hindered the photocatalytic activity.

Acknowledgements

This work was partially supported by the 973 Program (no. 2014CB239301), China, Collaborative Innovation Center of Chemical Science and Engineering (Tianjin), China, World Premier International Research Center Initiative on Materials Nanoarchitectonics (MANA), Japan and Japan Society for the Promotion of Science, Japan

Notes and references

Electronic Supplementary Information (ESI) available: Experimental, Thermogravimetric Analysis, photocatalytic activities, SEM, and XRD

1. Y. Bi, S. Ouyang, N. Umezawa, J. Cao and J. Ye, *J. Am. Chem. Soc.*, 2011, 133, 6490-6492.
2. G. Xi and J. Ye, *Chem. Commun.*, 2010, 46, 1893-1895.
3. J. Jiang, K. Zhao, X. Xiao and L. Zhang, *J. Am. Chem. Soc.*, 2012, 134, 4473-4476.
4. G. Liu, J. C. Yu, G. Q. Lu and H.-M. Cheng, *Chem. Commun.*, 2011, 47, 6763-6783.
5. B. P. Bastakoti, N. L. Torad and Y. Yamauchi, *ACS Appl. Mater. Interfaces*, 2014, 6, 854-860.
6. M. Zhao, H. Xu, H. Chen, S. Ouyang, N. Umezawa, D. Wang and J. Ye, *J. Mater. Chem. A*, 2015, 3, 2331-2337.
7. B. P. Bastakoti, Y. Li, M. Imura, N. Miyamoto, T. Nakato, T. Sasaki and Y. Yamauchi, *Angew. Chem. Int. Ed.*, 2015, 127, 4296-4299.
8. J. Yang and J. H. Swisher, *Mater. Charact.*, 1996, 37, 153-159.
9. J. C. Conesa, *Catal. Today*, 2013, 208, 11-18.
10. A. A. Gribb and J. F. Banfield, *Am. Mineral.*, 1997, 82, 717-728.
11. H. Xu and L. Zhang, *J. Phy. Chem. C*, 2009, 113, 1785-1790.
12. S. Yuan, J. Mu, R. Mao, Y. Li, Q. Zhang and H. Wang, *ACS Appl. Mater. Interfaces*, 2014, 6, 5719-5725.
13. K. Pan, Y. Dong, W. Zhou, Q. Pan, Y. Xie, T. Xie, G. Tian and G. Wang, *ACS Appl. Mater. Interfaces*, 2013, 5, 8314-8320.
14. E. García-Ramírez, M. Mondragón-Chaparro and O. Zelaya-Angel, *Appl. Phys. A*, 2012, 108, 291-297.
15. R. Liu, H. Ye, X. Xiong and H. Liu, *Mater. Chem. Phys.*, 2010, 121, 432-439.
16. M. Agrawal, S. Gupta, A. Pich, N. E. Zafeiropoulos and M. Stamm, *Chem. Mater.*, 2009, 21, 5343-5348.
17. C. Ye, S. S. Pan, X. M. Teng, H. T. Fan and G. H. Li, *Appl. Phys. A*, 2007, 90, 375-378.
18. F. H. DullN and D. E. Rase, *J. Am. Ceram. Soc.*, 1960, 43, 125-131.
19. J. Zhang, Q. Xu, Z. Feng, M. Li and C. Li, *Angew. Chem. Int. Ed.*, 2008, 47, 1766-1769.
20. E. S. Toberer, J. D. Epping, B. F. Chmelka and R. Seshadri, *Chem. Mater.*, 2006, 18, 6345-6351.
21. H. J. Fan, Y. Yang and M. Zacharias, *J. Mater. Chem.*, 2009, 19, 885-900.
22. Z. Hong, M. Wei, Q. Deng, X. Ding, L. Jiang and K. Wei, *Chem. Commun.*, 2010, 46, 740-742.

23. Y. Qu, W. Zhou, Z. Ren, G. Wang, B. Jiang and H. Fu, *ChemCatChem*, 2014, 6, 2258-2262.
24. B. P. Bastakoti, S. Ishihara, S. Y. Leo, K. Ariga, K. C. Wu and Y. Yamauchi, *Langmuir*, 2014, 30, 651-659.
25. Y. Li, B. P. Bastakoti, M. Imura, S. M. Hwang, Z. Sun, J. H. Kim, S. X. Dou and Y. Yamauchi, *Chem. Eur. J.*, 2014, 20, 6027-6032.
26. B. P. Bastakoti, Y. Li, T. Kimura and Y. Yamauchi, *Small*, 2015, 11, 1992-2002.
27. H. Zhang and J. F. Banfield, *J. Phy. Chem. B*, 2000, 104, 3481-3487.
28. C.-L. Wang, W.-S. Hwang, K.-M. Chang, H.-H. Ko, C.-S. Hsi, H.-H. Huang and M.-C. Wang, *Int. J. Mol. Sci.*, 2011, 12, 935-945.
29. C.-L. Wang, W.-S. Hwang, H.-H. Ko, C.-S. Hsi, K.-M. Chang and M.-C. Wang, *Metall. Mater. Trans. A*, 2013, 45, 250-260.

Graphical Abstract

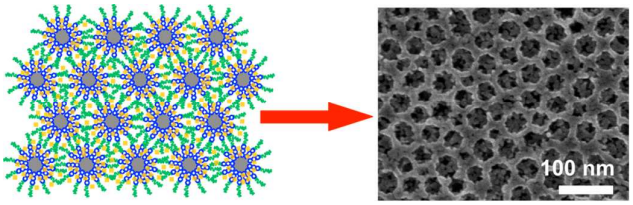

Ming Zhao, Bishnu Prasad Bastakoti*, Yunqi Li, Hua Xu, Jinhua Ye, Zongwen Liu, and Yusuke Yamauchi*

A hybrid mesoporous $TiO_2/Zn_2Ti_3O_8$ film synthesized by polymeric micelles assembly approach